Superalloys 2012: 12th International Symposium on Superalloys
Edited by: Eric S. Huron, Roger C. Reed, Mark C. Hardy, Michael J. Mills, Rick E. Montero, Pedro D. Portella, Jack Telesman
TMS (The Minerals, Metals & Materials Society), 2012

Dendrite bending during directional solidification

J.W. Aveson[1,*], G. Reinhart[2,3], H. Nguyen-Thi[2,3], N. Mangelinck-Noël[2,3], A. Tandjaoui[2,3], B. Billia[2,3], K. Goodwin[4], T.A. Lafford[5], J. Baruchel[5], H.J. Stone[1] and N. D'Souza[4]

[1]Rolls-Royce University Technology Centre, Department of Materials Science and Metallurgy, University of Cambridge, Pembroke Street, Cambridge, CB2 3QZ, United Kingdom
[2]Aix Marseille Univ & [3]CNRS, IM2NP UMR 7334 Campus Saint-Jerome, Case 142 13397 Marseille Cedex 20, France
[4] Rolls-Royce plc., PO Box 31, Derby, DE24 8BJ, United Kingdom,
[5] European Synchrotron Radiation Facility, 6 Rue Jules Horowitz, BP220, 38043 Grenoble Cedex 9, France

Keywords: solidification, dendrites, X-ray imaging, CMSX-4, electron backscattered diffraction

Abstract

In order to ascertain the origin of deformation and sub-grains in single crystal castings, an *in situ*, time-resolved X-ray radiographic imaging experiment was performed at the BM05 beam line of the European Synchrotron Radiation Facility (ESRF). This provided direct experimental evidence of the origin of crystallographic misorientation during the directional solidification of the nickel-based superalloy CMSX4. Solidification monitoring revealed that dendrites deform by bending and possibly torsion, and with deformation occurring early during dendrite growth, influencing the establishment of the dendritic array. These observations were related with electron backscattered diffraction data from *ex situ* samples. The bending and torsion contributions to deformation were extracted from the electron backscattered diffraction data using a data analysis scheme capable of isolating the deformation modes. In the component tested, bending was identified as the predominant deformation mode in sub-grain formation, but torsion effects were also seen to be significant.

Introduction

60 years of development in nickel-based superalloys has been driven by the need for higher temperature capability in gas turbine engines. Improvements in casting and solidification processing have led to the routine production of large single crystals of Ni-based alloys. In producing such single crystal turbine blades, any phenomena that lead to the introduction of grain boundaries must be avoided. During solidification, grain boundaries can be introduced through dendrite deformation or fragmentation, or nucleation ahead of the growth front. The underlying mechanisms of dendrite deformation and fragmentation remain poorly understood, owing to the difficulty of experimental observation, and the fact it is a multiphysics problem with coupling of phase equilibria, fluid mechanics, and mechanical behaviour.

'*Post mortem*' analyses of solidified samples of increasingly sophisticated techniques have provided important insights into deformation during solidification of superalloys. For example, the use of X-ray topography has provided new information on the occurrence of deformation and misorientation in single crystal dendritic solidification of Ni-based superalloys [1–3]. Similarly, in recent years, electron backscattered diffraction (EBSD) has come to provide a routine, yet powerful tool, for the detailed charaterisation of material microstructures [4, 5]. It has been used in nickel-based superalloy castings to investigate cumulative misorientations in re-entrant components [6], and for the identification of subgrains in the melt-back region of seeded single-crystal castings [7,8]. In most of these studies, the reasons for the development of misorientations were either not addressed, or suggested to be the result of plastic deformation occurring in order to relieve residual stresses. Amongst these studies, D'Souza *et al.* [6] concluded that misorientation developed through branching and growth within the dendrite mush. This has motivated the present study based on the application of *in situ* synchrotron radiographic imaging to the problem of deformation during solidification.

X-ray imaging of solidification was initiated by the experiments of Stephenson and Beech [9, 10] and in the last decade has made a significant impact on solidification research with the advent of *in situ*, time resolved imaging using synchrotron radiation [11]. Particular research highlights have been the study of the role of solute build-up on remelting-driven fragmentation [12], the observa-

tion of misorientations emerging during solidification [13, 14], imaging eutectic solidification [15, 16] and identifying the importance of granular behaviour in semi-solid alloys [17].

Until recently, *in situ* solidification experiments were confined to low temperature systems such as Pb-Sn and aluminium based alloys owing limitations in the temperature capability of the furnaces available [18, 19]. In addition, studies were typically limited to binary alloys. Recently, two furnaces have come online that enable higher temperature systems to be investigated: one facility is installed at the SPring8 synchrotron in Japan, which has been successfully used for imaging steel solidification [20,21], and one at the European Synchrotron Radiation Facility, which has been used for characterising silicon solidification and for the present study. This important development now allows for detailed examination of the processing of industrially important materials where the added value depends crucially on the careful control of solidification processing.

Theoretical studies of dendrite deformation and fragmentation have broadly concluded that remelting processes are of principal importance [24–26]. Dendrites appear to be only susceptible to flow-induced plastic deformation during rapid solidification, owing to the fine length-scales and relatively large skin pressures involved [27]. However, elastic stresses may also play a role in phase equilibria causing remelting [28].

Experimental studies of dendrite deformation and fragmentation are relatively limited. Transparent materials that freeze like metals have been used with some success: the Copley experiment gives an excellent example of the application to single crystal castings [29, 30]. However, the influence of flow on fragmentation behaviour is difficult to assess owing to the conflicting requirements for clear imaging and imposable flow conditions [31, 32]. Fragmentation has been observed under remelting conditions in transparent alloys [33, 34] and X-ray imaging experiments on aluminium alloys have shown the importance of solutal effects on fragmentation of tertiary dendrite arms [12]. Localised deformation due to body forces and torques has also been reported through the use of X-ray diffraction topography [13, 14]. Furthermore, certain systems have shown a 'cascade fragmentation' effect which may be of considerable importance where channel convection flow fields are set up between primary dendrite arms [35].

In this study, deformation and crystallographic misorientation during directional solidification of

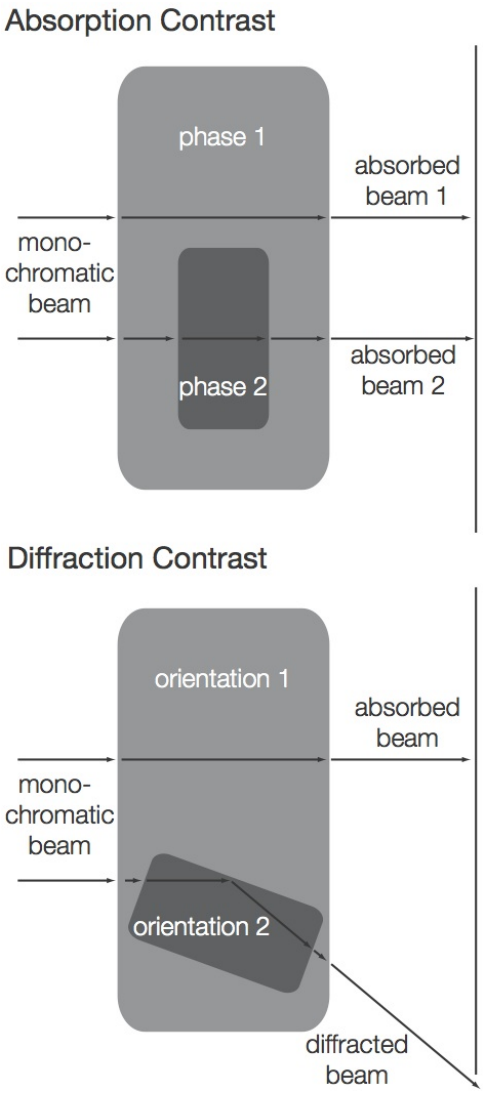

Figure 1: Schematic illustration of the two contrast modes in X-ray imaging used in this study: a. absorption contrast, after Li *et al.* [22]. Diffraction contrast, where the dark grey region is oriented at the Bragg condition relative to the incoming photon beam. After Authier [23].

CMSX4 was performed using X-ray radiography with two complementary contrast modes: absorption contrast and diffraction contrast. These are summarised in Figure 1. Absorption contrast maps the through-thickness attenuation owing to differences in elemental composition and density. Diffraction contrast occurs when a region is well-oriented with respect to the incoming beam such that the Bragg condition is met. This results in an extinction in the transmitted image, identify-

ing the region where a crystal meets the Bragg diffraction condition. To support the observations made using X-ray imaging, EBSD of directionally solidified CMSX4 samples was also conducted. In order to obtain data pertinent to the assessment of the alignment of cast components, an electron backscatter diffraction analysis routine was developed capable of separately quantifying the bending and rotation modes from EBSD data.

Experiments

X-ray imaging

In situ X-ray imaging was carried out at the European Synchrotron Radiation Facility (ESRF) on the BM05 beam line. A specimen of CMSX4 was cut to 40mm × 6mm × 0.3mm and polished using diamond suspension down to 0.25μm. This specimen was mounted in a BN crucible and placed in a bespoke AET Technologies Bridgman furnace. The specimen was completely melted before controlled cooling was carried out. Images were recorded at a frequency of 0.2 Hz on a Fast Readout Low Noise (FReLoN) camera developed by the ESRF.

Electron backscattered diffraction

For the electron backscattered diffraction, a specimen was produced by casting a component with a narrow constriction similar to that described by D'Souza *et al.* [36]. A seed was melted back before being grown through the constriction into the blade geometry. This was cross-sectioned through the constriction, before being mounted, ground and polished using a protocol culminating in polishing with colloidal silica. The specimen was mounted in a CamScan MX-2600 SEM fitted with an Oxford Instruments EBSD system. An acceleration voltage of 25 keV was used at a specimen tilt of 70°. A map was recorded with a step size of 2.5μm and automated indexing was used to return the Euler angles, $\theta_1, \theta_2, \theta_3$.

Results

X-ray imaging

Figures 2 shows a large grain observed during the radiography experiment. This grain nucleated at position a. and rapidly grew out to form the observed structure. The dendrites are very needle-like compared with other studies such as [37]. This is likely to be due to the comparatively fast solidification conditions experienced in the experiment, leading to fast tip velocities and small dendrite tip radii, and consequentially narrow trunk diameters. The dendrite are spacing can be seen to vary across the field of view being finer towards the bottom of the image compared with the top. This may be attributed to the temperature profile across the sample which was such that the top of the sample was maintained at a higher temperature than at the bottom of the sample. As such, following the nucleation event at position a., the dendrite was able to grow into increasingly undercooled liquid towards the bottom of the field of view. Therefore, the primary dendrite arm spacing through this region is thinner in this region that towards the top of the field of view. The darker globular features are likely to be secondary dendrite arms in the thickness of the specimen.

The strongly absorbing W and Re segregate heavily to the dendrite cores in this alloy [38]. Combined with this, the fact that back diffusion is slow compared to the dendrite growth velocity suggests that it is possible that the very fine dendrites observed may be, in part, attributed to the preferential X-ray absorption of the dendrite cores, rather than the limit of the solid liquid interface. However, it seems more plausible that the dendrites genuinely are remarkably thin as a result of the rapid growth under a high degree of undercooling. At position b., a primary stem is seen to be blocked by a tertiary dendrite arm. It can be seen that the dendrites do not actually touch, demonstrating that this has occurred as a result of solutal impingement. At position c., a dendrite is identified that has bent through approximately 5°. This bent dendrite has continued to grow and indeed subsequently blocked the growth of the adjacent dendrite. It is clear that this spontaneous bending would lead to the formation of a grain boundary in the final component.

Figure 3 shows a dendrite imaged by extinction contrast where a small region of the dendrite is in the Bragg diffraction condition. A black region is seen to progressively descend the dendrite arm with time. This extinction spot can be seen to appear and disappear, revealing that the deformation is elastic, which could be bending or torsional in nature. Whilst superposition of these images shows that there is no perceptible bending in the plane of the image, bending may indeed be occurring with some displacement component out of the plane of the image. From the present extinction contrast radiography it is not possible to unanimously state whether this dynamic, elastic deformation is bending or torsion, or some combination of the two de-

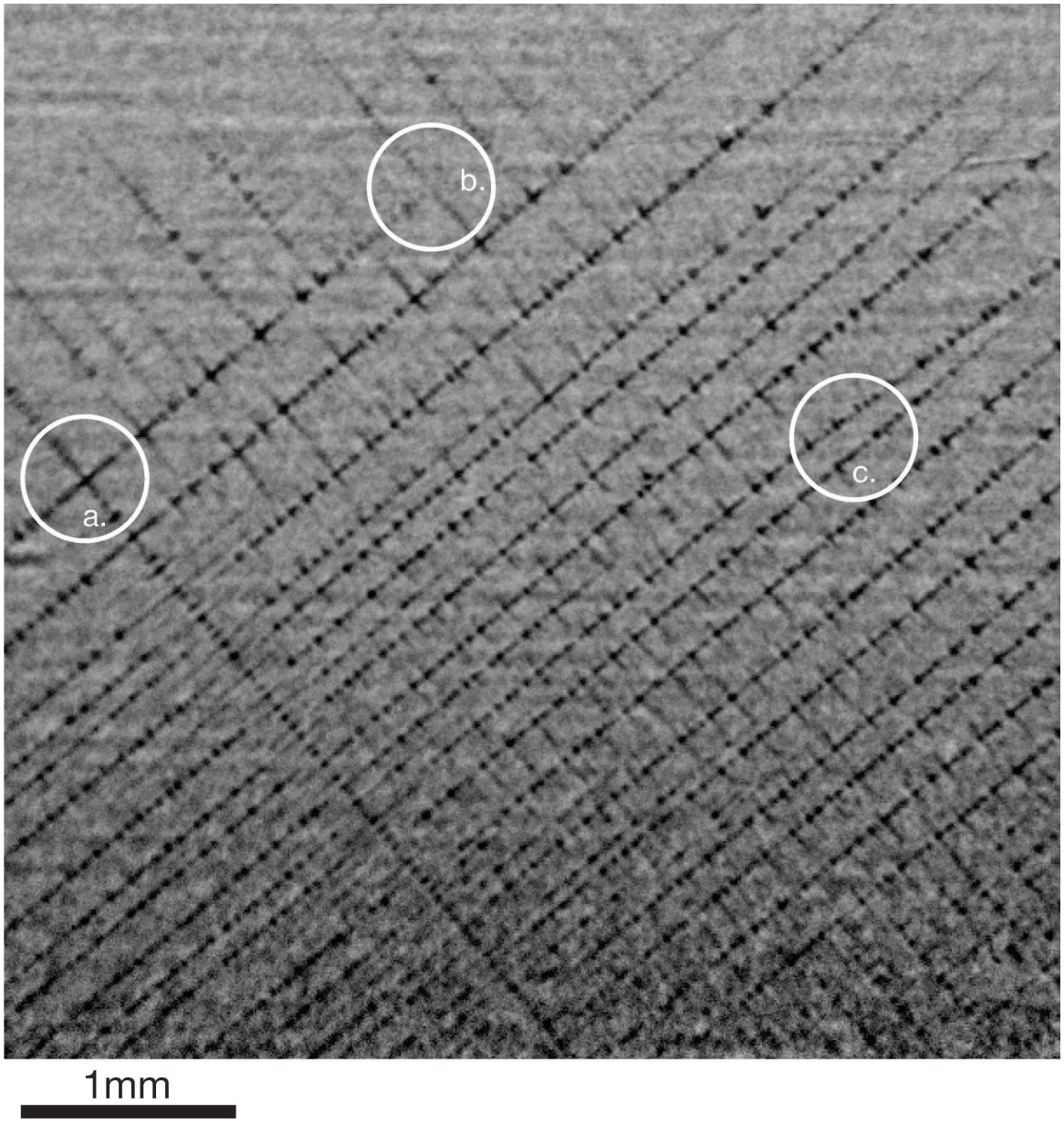

Figure 2: Radiograph of solidifying CMSX4. The figure shows a grain that nucleated at site a. Location b. shows the solutal blocking of a primary dendrite arm by a tertiary dendrite arm. Location c. shows the position of a bent dendrite arm that blocks the growth of an adjacent dendrite arm. Assuming that the dendrites that survive out to the top right hand corner would form primary dendrites in a cast component, a linear intercept estimate of primary dendrite arm spacing gives an value of $\lambda_{\mathrm{PDAS}} = 255\mu m$.

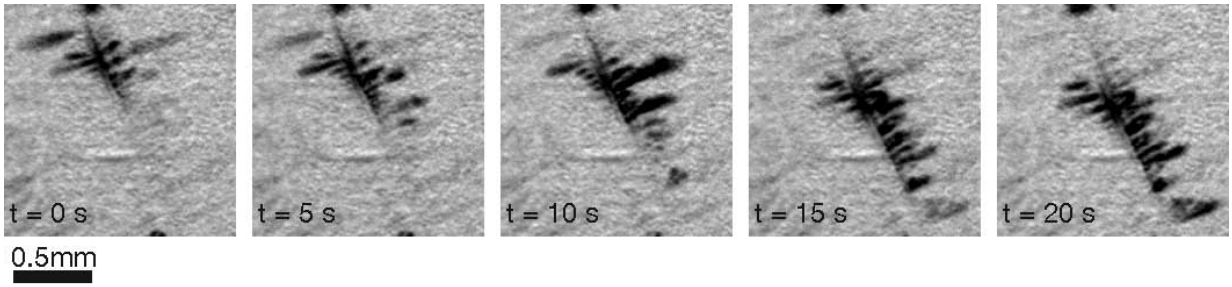

Figure 3: Series of radiographs showing the deformation of a dendrite arm. The black region is an extinction where the dendrite backbone and secondary arms are oriented with respect to the incoming beam such that the beam is diffracted out of the direct radiograph. The motion of the black region strongly suggests that the dendrite is undergoing dynamic elastic deformation.

formation modes. It is thus necessary to employ electron backscattered diffraction in order to distinguish between these deformation modes.

EBSD data analysis routine

The raw electron backscattered diffraction data showed a relatively uniform distribution in the second Euler angle, θ_2 and a pronounced difference between dendritic and interdendritic material in the first and third Euler angles, θ_1 and θ_3. However, whilst the Euler angles do uniquely describe the orientation of the crystal and are straightforward to comprehend, they are less useful for detailed calculations owing to their interdependency, and so a novel approach was designed in order to map the angles of bending and torsion away from the average orientation. The rotations described by the Euler angles were converted to quaternions, reduced to the fundamental zone by the methods of Sutton & Balluffi [39] and the average orientation calculated by the methods of Glez & Driver [40]. Denoting a right-handed Cartesian set describing the average orientation as $\bar{\mathbf{e}}$ such that $\bar{\mathbf{e}}_3$ is the growth direction of the seed, and the superscript i represents the i^{th} measurement, the bending angle is:

$$\theta_{\text{bending}} = \arccos\left(\mathbf{e}_3^i \cdot \bar{\mathbf{e}}_3\right) \tag{1}$$

Subsequently, applying a rotation through an angle θ_{bending} about an axis in the direction $\mathbf{u} = \mathbf{e}_3^i \times \bar{\mathbf{e}}_3$ brings the $\mathbf{e}_3$ axes of the two basis sets to coincidence. For the purpose of the present computation, this was carried out by generating the rotation matrix that corresponds to an axis-angle rotation about an axis $\mathbf{u}$ through an angle θ which is concisely written as [42]

$$R_{ij} = \delta_{ij}\cos\theta + \epsilon_{ijk}u_k\sin\theta + (1-\cos\theta)\,u_iu_j \tag{2}$$

where i,j and k are dummy suffices, δ_{ij} is the Kronecker delta, ϵ_{ijk} is the Levi-Civita symbol and the Einstein summation convention has been used. When the basis set $\mathbf{e}_3^i$ is transformed by $\mathbf{R}$, which is an axis-angle rotation about $\mathbf{u}$ through θ_{bending}, then the vectors $\bar{\mathbf{e}}_3$ and $\mathbf{R}\mathbf{e}_3^i$ are co-incident and the angle of torsion can be readily determined as

$$\theta_{\text{torsion}} = \arccos\left(\mathbf{R}\mathbf{e}_3^i \cdot \bar{\mathbf{e}}_1\right) \tag{3}$$

which is equivalent to the same scalar product being taken between the $\mathbf{e}_2$ axes and indeed offers a check for equivalency.

The maps produced using this method are shown in Figure 4 along with a backscattered electron image of the same region. It can be seen that the sub-grain boundary that approximately bisects the map emerges largely from differences in bending angle. Furthermore, the dendritic morphology can be seen in the bending and torsion angles, showing that the dendrite and the interdendritic material do not share a common orientation. The extended sub-grain at the base of the image differs from the sub-grain in the centre of the image and is formed by both bending and torsion. There is also a sub-grain to the left hand side of that has formed solely through torsion.

The distribution of bending and torsion angles can be plotted as histograms (Figure 5). This reveals the extent to which the bending of dendrites leads to the formation of sub-grains. The distribution of bending angles is sharply trimodal, indicating that sub-grain formation is defined by dendrite

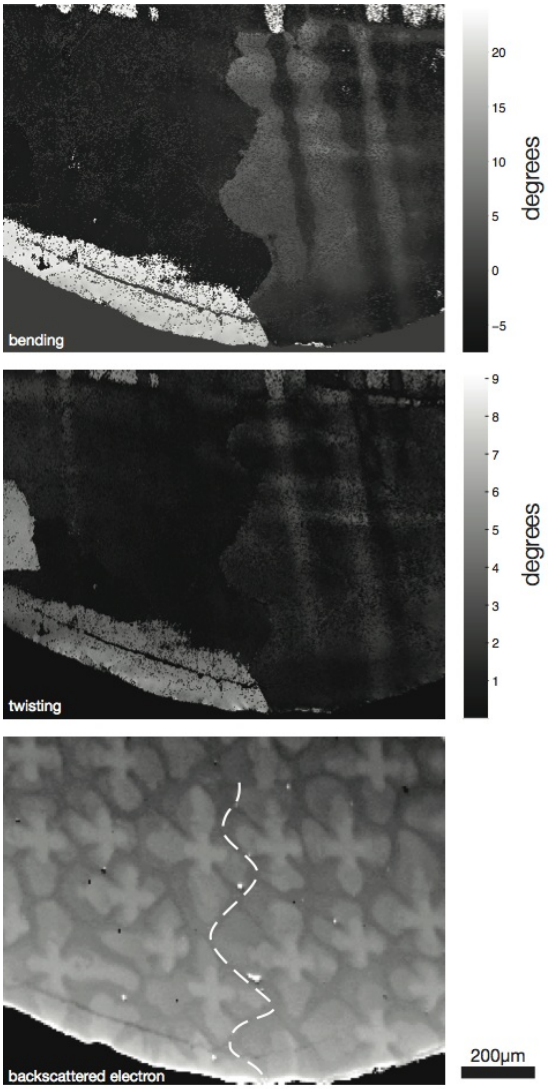

Figure 4: Maps of dendrite bending angle (top frame), dendrite torsion angle (middle frame) and a backscattered electron image of the same region. Angles in degrees. Primary dendrite arm spacing calculated using the method of Warnken & Reed $\lambda_{\mathrm{PDAS}} = 223\mu m$ [41]

bending. However, the distribution of torsion angles is closer to being continuous, demonstrating that the sub-grains could not have formed by fragmentation or nucleation.

Discussion

The relative importance of torques and bending moments on deformation during solidification is currently an active area in solidification research and is clearly of great pertinence to single crystal castings in the foundry. In the X-ray images, dendrites were observed that had been deformed, clearly under bending and possibly with some torsional contribution. The present EBSD results suggest that bending is predominantly important, but that torsion in not negligible. As previously observed by Stanford *et al.*, incidences of stray grains in melt-back regions typically occur at the periphery of the casting [7,8], although these stray grains were randomly oriented. In that case, prior secondary dendrite arms could fragment via remelting instabilities, explaining the stray grains. In the present study, the constriction is designed that dendrites growing in the seed direction overgrow nucleated or fragmented stray grains [8]. Indeed, this is supported by the continuity of the distribution of torsion angle in the histogram in Figure 5. Thus, in the present geometry, sub-grain formation can

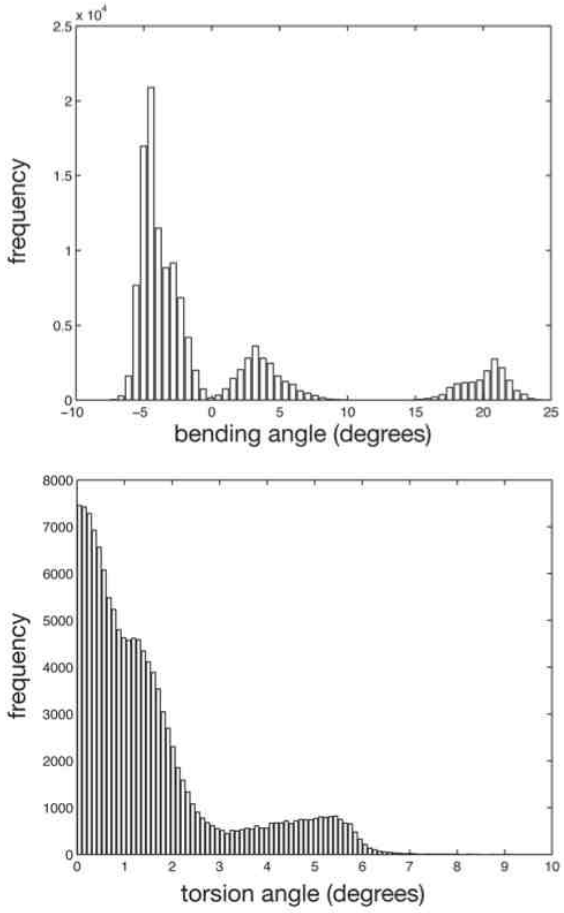

Figure 5: Bending and torsion angles binned and plotted as histograms.

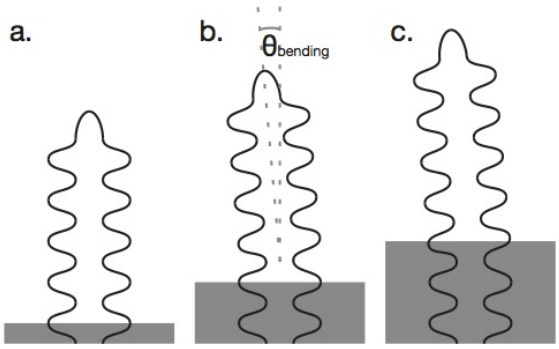

Figure 6: Schematic demonstrating the locking-in of spontaneous localised elastic deformation. Figure 6a. shows a dendrite growing in an undeformed state with the interdendritic front trailing the dendrite tips. Figure 6b. shows a spontaneous bending that has occurred ahead of the interdendritic front, such as in Figure 3. Figure 6c. shows how the interdendritic front can freeze in a misorientation, resulting in the dendritic morphology being observed in the EBSD maps in Figure 4.

be posited to be a result of the impingement of the dendrite on the mould wall.

Some exploration of the origin of bending moments and torques is necessary, which from the present evidence must be somewhat putative. It can be considered that since sub-grain formation at casting peripheries is common, the constraint of the mould must play a key role. In a directional casting, thermal contraction produces a relative downward motion of the casting. If the solid is not constrained, the dendrite is free to move without deformation in the direction of contraction. However, if constraint occurs either by adhesion to the mould wall or from a secondary dendrite arm in a re-entrant component, then a bending moment will arise. If the primary dendrite growth direction is parallel to the heat flow axis ($\nabla T \cdot \mathbf{e}_3 = 0$) then the primary dendrite arm will not experience a bending moment from constraint effects. Torques can only arise through inequality in the forces experienced by opposing dendrite arms: similarly, the condition for torsion-free bending of dendrites will be that a secondary dendrite arm lies in the direction $\nabla T \times \mathbf{e}_3$. However, a fuller experimental campaign and finite element simulations will be necessary in order to fully determine the relative importance of these effects.

Figure 4 shows a disparity between the orientation of the dendrite and that of the interdendritic material. This implies that the interdendritic material freezes with the orientation of the solid below it rather than the dendrite adjacent to it when the dendrite has bent or is twisted. Thus, we identify that sub-grains can form by both elastic and plastic deformation:

plastic deformation: the deformed dendrite impinges on an adjacent dendrite, forming a low angle grain boundary. This can readily be envisaged in the situation shown in Figure 2.

elastic deformation: the deformation occurs ahead of the interdendritic solid/liquid interface such as the deformation shown in Figure 3. The interdendritic material then freezes in such a manner that the elastic deformation becomes locked in, by freezing with the orientation of the advancing interdendritic front. This is demonstrated schematically in Figure 6. This process would result in a misorientation between the dendrite and the interdendritic material, as exhibited in Figure 4.

It is clear from Figures 2 & 3 that the dendrites of CMSX4 seem very slender and needle-like, when compared against, for instance, similar images from Al-Cu alloys [43] or NH_4Cl-H_2O solutions [25]. It is important to note that solidification conditions differ between each of the images: yet the primary dendrite arm spacings are comparable between Figure 2 and Figure 4 suggesting a similar product $G^{-1/2}v^{-1/4}$ [44]. However, a progression in morphology can be seen through Figures 2 - 4. Figure 2 shows very needle-like crystals at fast, early stage solidification, through to more rounded secondary dendrite arms with a sharp backbone (Figure 3), with the classic, more rounded morphologies seen in Figure 4. The freezing range is relatively long - differential scanning calorimetry suggest approximately 60K [45], giving ample time for coarsening under typical casting conditions. These observations therefore open the prospect of formulating and investigating potential correlations between dendrite morphology and defects.

Conclusions

In summary, *in situ* time resolved X-ray imaging offers the possibility of obtaining unique insights into transient growth processes in solidification of Ni-based superalloys. Furthermore, an approach by which bending and torsion of dendrites may be discriminated from EBSD data has been developed

and allows quantitative data to be obtained. Further work is necessary in order to understand the interaction between mould geometry and the deformation observed in terms of the torque and bending moment experienced by the dendrite.

Acknowledgements

The authors are grateful to the European Synchrotron Radiation Facility for the provision of beam time on the BM05 beam line and to Rolls-Royce plc. for provision of material for the study. X. Guichard is particularly acknowledged for his technical assistance at BM05. S. Griggs, H. Mathur and O.M.D.M. Messé are acknowledged for assistance with the acquisition of the EBSD data.

J.W.A. is grateful to the EPSRC and Rolls-Royce plc. for the provision of a studentship under the EPSRC/Rolls-Royce plc. Strategic Partnership.

References

[1] M. Rappaz and E. Blank. Combined X-ray microdiffraction and topography experiment for microstructural analysis of heterogeneous materials. *Journal of Materials Science*, 22:896–906, 1987.

[2] R.E. Napolitano and R.J. Schaefer. The convergence-fault mechanism for low-angle boundary formation in single-crystal castings. *Journal of Materials Science*, 35:1641, 2000.

[3] N. Siredey, M. Boufoussi, S. Denis, and J. Lacaze. Dendritic growth and crystalline quality of nickel-base single grains. *Journal of Crystal Growth*, 130:132, 1993.

[4] V. Randle. Applications of electron backscatter diffraction to materials science: status in 2009. *Journal of Materials Science*, 44:4211, 2009.

[5] A.J. Wilkinson. Assessment of lattice strain, rotation and dislocation content using electron back-scatter diffraction. *Journal of Physics: Conference Series*, 326:012004, 2011.

[6] N. D'Souza, M. Newell, K. Devendra, P.A. Jennings, M.G. Ardakani, and B.A. Shollock. Formation of low angle grain boundaires in Ni-based superalloys. *Materials Science and Engineering A*, 413-414:567–570, 2005.

[7] N. Stanford, A. Djakovic, B. Shollock, M. McLean, N. D'Souza, and P. Jennings. Defect grains in the melt-back region of CMSX-4 single crystal seeds. In K.A. Green, T.M. Pollock, H. Harada, T.E. Howson, R.C. Reed, J.J. Schirra, and S. Walston, editors, *Superalloys 2004*. The Minerals, Metals and Materials Society, 2004.

[8] N. D'Souza, P.A. Jennings, X.L. Yang, H.B. Dong, P.D. Lee, and M. McLean. Seeding of single-crystal superalloys - role of constitutional undercooling and primary dendrite orientation on stray-grain nucleation and growth. *Metallurgical and Materials Transactions B*, 36:657, 2005.

[9] E.W.J. Miller and J. Beech. In situ radiographic observations of alloy solidification. *Metallography*, 5:298–300, 1972.

[10] E.W.J. Miller, M.P. Stephenson, and J. Beech. A technique for the direct observation of alloy solidification. *Journal of Physics E: Scientific Instruments*, 8:33–37, 1975.

[11] M. Asta, C. Beckermann, A. Karma, W. Kurz, R. Napolitano, M. Plapp, G. Purdy, M. Rappaz, and R. Trivedi. Solidification microstructures and solid-state parallels: recent developments, future directions. *Acta Materialia*, 57:941–971, 2009.

[12] D. Ruvalcaba, R.H. Mathiesen, D.G. Eskin, L. Arnberg, and L. Katgerman. *In situ* observations of dendrite fragmentation due to local solute enrichment during directional solidification of an aluminium alloy. *Acta Materialia*, 55:4287–4292, 2007.

[13] B. Billia, N. Bergeon, H. Nguyen-Thi, H. Jamgotchian, J. Gastaldi, and G. Grange. Cumulative mechanical moments and microstructure deformation induced by growth shape in columnar solidification. *Physical Review Letters*, 93:126105, 2004.

[14] G. Reinhart, A. Buffet, H. Nguyen-Thi, B. Billia, H. Jung, N. Mangelinck-Noël, N. Bergeon, T. Schenk, J. Härtwig, and J. Baruchel. *In situ* and real time analysis of the formation of strains and microstructure defects during solidification of Al-3.5 wt pct Ni alloys. *Metallurgical and Materials Transactions A*, 39:865–874, 2008.

[15] G. Zimmermann, U. Hecht, M. Mathes, and R.H. Mathiesen. Time resolved x-ray imaging of eutectic cellular patterns evolving during solidification of ternary Al-Cu-Ag alloys. *International Journal of Materials Research*, 101:1484–1489, 2010.

[16] C.M. Gourlay, K. Nogita, A.K. Dahle, Y. Yamamoto, K. Uesugi, T. Nagira, M. Yoshiya, and H. Yasuda. In situ investigation of unidirectional solidification in Sn-0.7Cu and Sn-0.7Cu-0.06Ni. *Acta Materialia*, 59:4043, 2011.

[17] C.M. Gourlay, A.K. Dahle, T. Nagira, N. Nakatsuka, K. Nogita, K. Uesugi, and H. Yasuda. Granular deformation mechanisms in semi-solid alloys. *Acta Materialia*, 59:4933, 2011.

[18] R.H. Mathiesen, L. Arnberg, F. Mo, T. Weitkamp, and A. Snigirev. Time resolved x-ray imaging of dendritic growth in binary alloys. *Physical Review Letters*, 83:5062–5065, 1999.

[19] H. Nguyen-Thi, H. Jamgotchian, J. Gastaldi, J. Härtwig, T. Schenk, H. Klein, B. Billia, J. Baruchel, and Y. Dabo. Preliminary *in situ* and real-time study of directional solidification of metallic alloys by x-ray imaging techniques. *Journal of Physics D: Applied Physics*, 36:A83–A86, 2003.

[20] H. Yasuda, T. Nagira, M. Yoshiya, N. Nakatsuka, A. Sugiyama, K. Uesugi, and K. Umetani. Development of X-ray imaging for observing solidification of carbon steels. *ISIJ International*, 51:402–408, 2011.

[21] T. Nagira, C.M. Gourlay, A. Sugiyama, M. Uesugi, Y. Kanzawa, M. Yoshiya, K. Uesugi, K. Umetani, and H. Yasuda. Direct observation of deformation in a semi-solid carbon steel. *Scripta Materialia*, 64:1129, 2011.

[22] B. Li, H.D. Brody, and A. Kazimirov. Real time observation of dendrite coarsening in Sn-13wt pct Bi alloy by synchrotron microradiography. *Physical Review E*, 70:062602, 2004.

[23] A. Authier. *Dynamical theory of x-ray diffraction*. Oxford University Press, 2004.

[24] M. Rettenmayr. Melting and remelting phenomena. *International Materials Reviews*, 54:1–17, 2009.

[25] J. Pilling and A. Hellawell. Mechanical deformation of dendrites by fluid flow. *Metallurgical and Materials Transactions A*, 27:229–232, 1996.

[26] K. Dragnevski, A.M. Mullis, D.J. Walker, and R.F. Cochrane. Mechanical deformation of dendrites by fluid flow during the solidification of undercooled melts. *Acta Materialia*, 50:3743–3755, 2002.

[27] A.M. Mullis. Deformation of dendrites by fluid flow during rapid solidification. *Materials Science and Engineering A*, 304-306:245–249, 2001.

[28] S. Ananiev, P. Nikrityuk, and K. Eckert. Dendrite fragmentation by catastrophic elastic remelting. *Acta Materialia*, 57:657–655, 2009.

[29] S.M. Copley, A.F. Giamei, S.M. Johnson, and M.F. Hornbecker. The origin of freckles in unidirectionally solidified castings. *Metallurgical Transactions*, 1:2193–2204, 1970.

[30] S.S.L. Peppin, H.E. Huppert, and M.G. Worster. Steady-state solidification of aqueous ammonium chloride. *Journal of Fluid Mechanics*, 599:465–476, 2008.

[31] J.W. Aveson. Studying flow effects on dendrite fragmentation using Rayleigh-Bénard convection. *Materials Science and Technology*, dx.doi.org/10.1179/1743284711Y.0000000128, 2012.

[32] T. Li, X. Lin, and W. Huang. Morphological evolution during solidification under stirring. *Acta Materialia*, 54:4815–4824, 2006.

[33] T. Sato, W. Kurz, and K. Ikawa. Experiments on dendrite branch detachment in the succinonitrile-camphor. *Transactions of the Japan Institute of Metals*, 28:1012–1021, 1987.

[34] S. Liu, S.Z. Liu, and A. Hellawell. Mechanism of dendrite fragmentation in casting. In *Light Metals 1997*, 1997.

[35] H. Jung and N. Mangelinck-Noël and H. Nguyen-Thi and N. Bergeon and B. Billia and A. Buffet and G. Reinhart and T. Schenk and J. Baruchel. Fragmentation in an al-7wt%si alloy studied in real time by x-ray synchrotron techniques. *International Journal of Cast Metals Research*, 22:208, 2009.

[36] N.J. D'Souza, P.A. Jennings, and K. Devendra. Method and mould for casting articles with a pre-determined crystalline orientation. United States Patent 7449063, 2008.

[37] J. Madison, J. Spowart, D. Rowenhorst, L.K. Aagesen, K. Thornton, and T.M. Pollock. Modeling fluid flow in three-dimensional single crystal dendritic structures. *Acta Materialia*, 58:2864–2875, 2010.

[38] R.A. Hobbs, S. Tin, and C.M.F. Rae. A castability model based on elemental solid-liquid partitioning in advanced nickel-based single crystals superalloys. *Metallurgical and Materials Transactions A*, 36:2761, 2005.

[39] A.P. Sutton and R.W. Balluffi. *Interfaces in crystalline materials*. Oxford University Press, 1995.

[40] J.-C. Glez and J. Driver. Orientation distribution analysis in deformed grains. *Journal of Applied Crystallography*, 34:280, 2001.

[41] N. Warnken and R.C. Reed. On the characterization of directionally solidified dendritic microstructures. *Metallurgical and Materials Transactions A*, 42:1675, 2011.

[42] S.L. Altmann. *Rotations, quaternions and double groups*. Oxford Science Publications, 1986.

[43] A. Bogno, H. Nguyen-Thi, N. Bergeon, N. Mangelinck-Noël, T. Schenk, B. Billia, E. Boller, and J. Baruchel. Application of synchrotron x-ray imaging to the study of dendritic equiaxed microstructure formation in Al-Cu alloys. *Nuclear Instruments and Methods in Physics Research B*, 268:394–398, 2010.

[44] W. Kurz and D.J. Fisher. *Fundamentals of solidification*. Trans Tech, 1992.

[45] H. Mathur. Private communication, 2012.